Supporting information for

The different composites of cellulose nanocrystals with $_{D}$- or $_{L}$-Histidine

Zehao Gu, Mengfan Lu, Kai Feng and Zhaoxia Jin*

Department of Chemistry, Renmin University of China, Beijing, People's Republic of China 100872

Table of contents

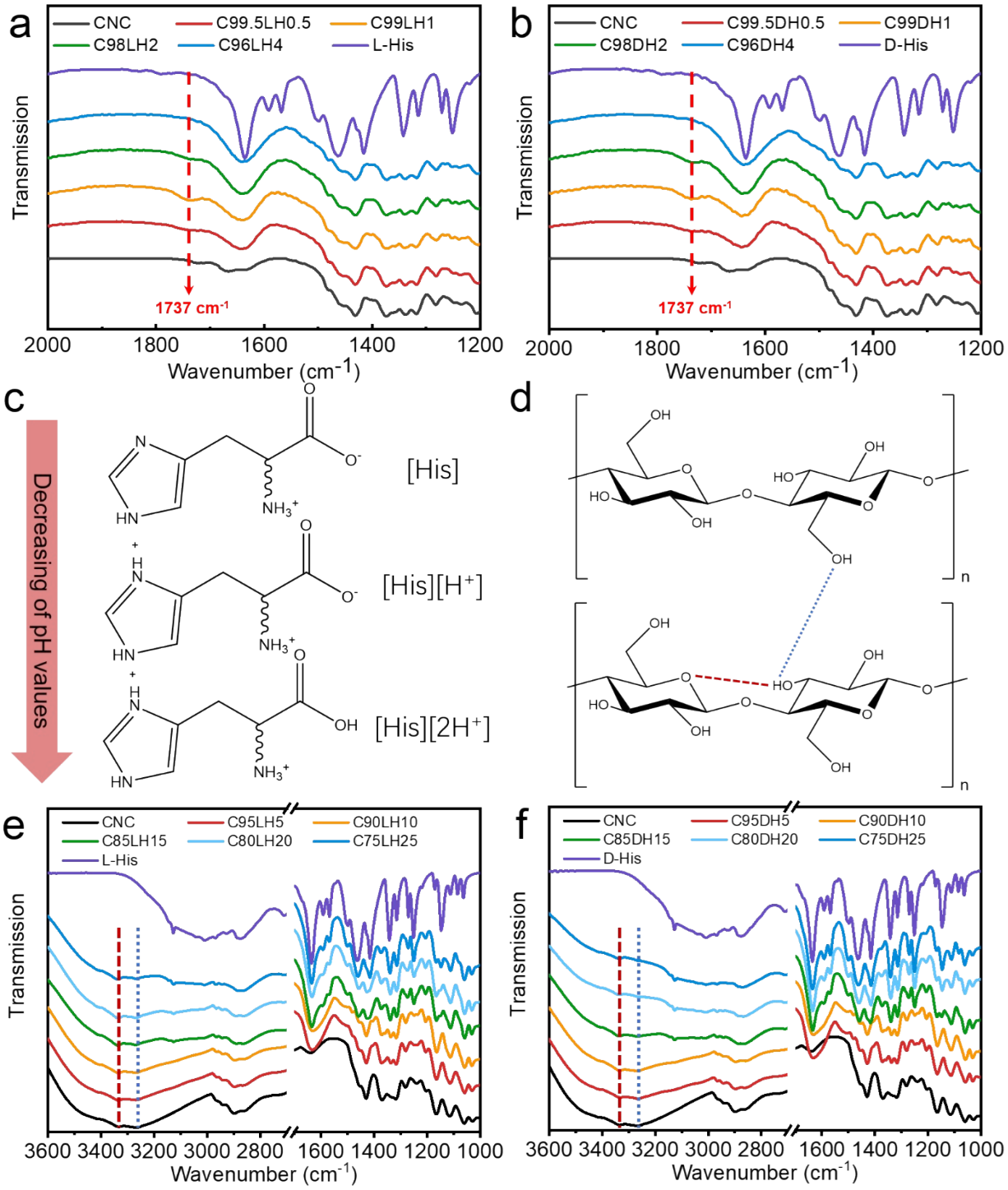

Figure S1. FTIR spectra for identifying the interactions of CNC/histidine hybrids. (a, b) Normalized FTIR spectra for CNC and CNC/histidine composite films at low concentrations of histidine in the $_{L}$- configuration (a) and $_{D}$-configuration (b). The transmission peak around 1737 cm^{-1} raised when the content of histidine increased from 0.5 wt.% to 2 wt.% (Figure S1a, S1b), which was assigned to the stretching vibration from the carboxyl of $[His][2H^{+}]$[1], indicating that the sulfonic acid group originally grafted on CNC was neutralized by histidine. (c) Proposed structures of the different protonation states of histidine in aqueous solution at changing pH value.[2] In the neutralized

condition, histidine stays at zwitterion form. With the increasing concentration of protons, protons are caught by the imidazole ring of a histidine, then named as [His][H^+]. Further decreasing of pH value results in that the side group of carboxylate transforms into carboxyl in the second protonation stage. (d) Schematic illustration of the intermolecular hydrogen bonding of cellulose. (e, f) Normalized FTIR spectra for CNC and CNC/histidine composite films at high concentrations of histidine, $_L$-His series (e), and $_D$-His series (f), respectively. The transmission bands around 3340 and 3285 cm^{-1} were assigned to the intramolecular hydrogen bonds (red dash line in Figure S1d) and the intermolecular hydrogen bonds (blue dash line in Figure S1d) based on literature[3].

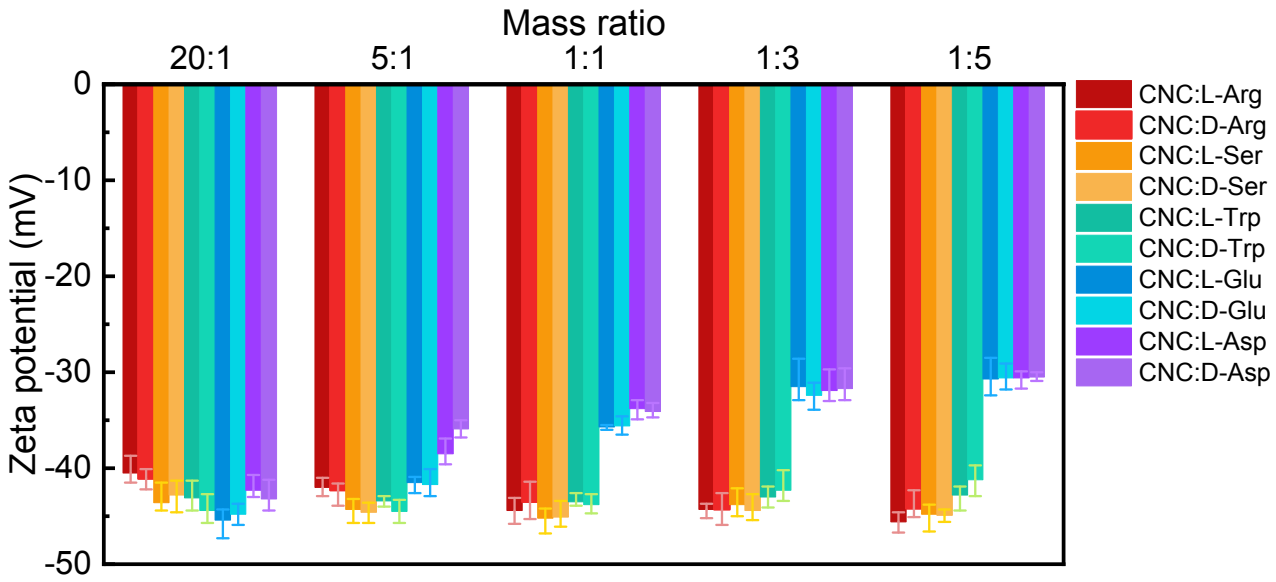

Figure S2. Zeta potential values for CNC/amino acid mixture suspensions with a varying weight ratio of CNCs to the amino acid.

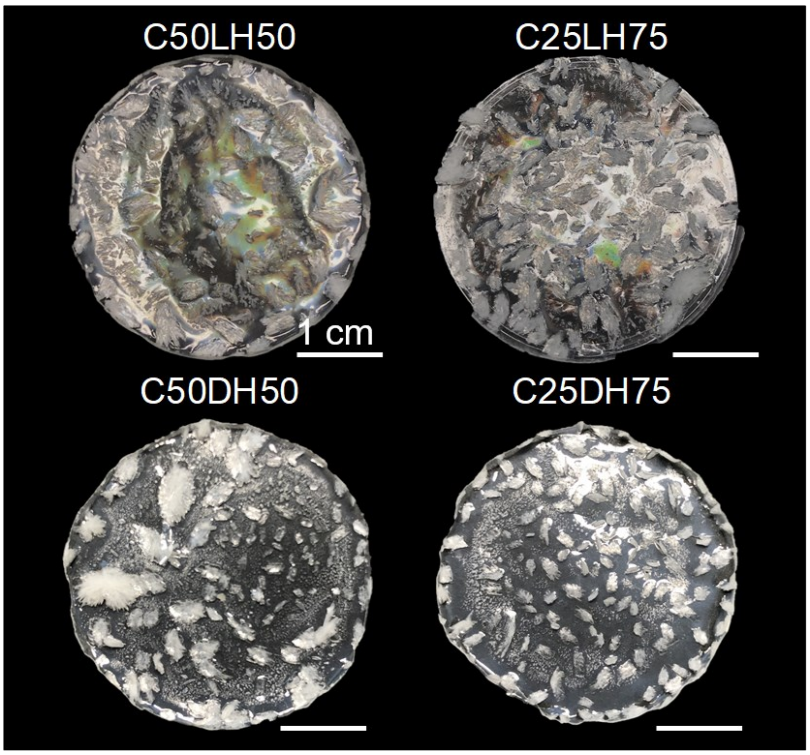

Figure S3. Photographs of hybrid samples: C50LH50, C25LH75, C50DH50, C25DH75. All scale bars are 1 cm.

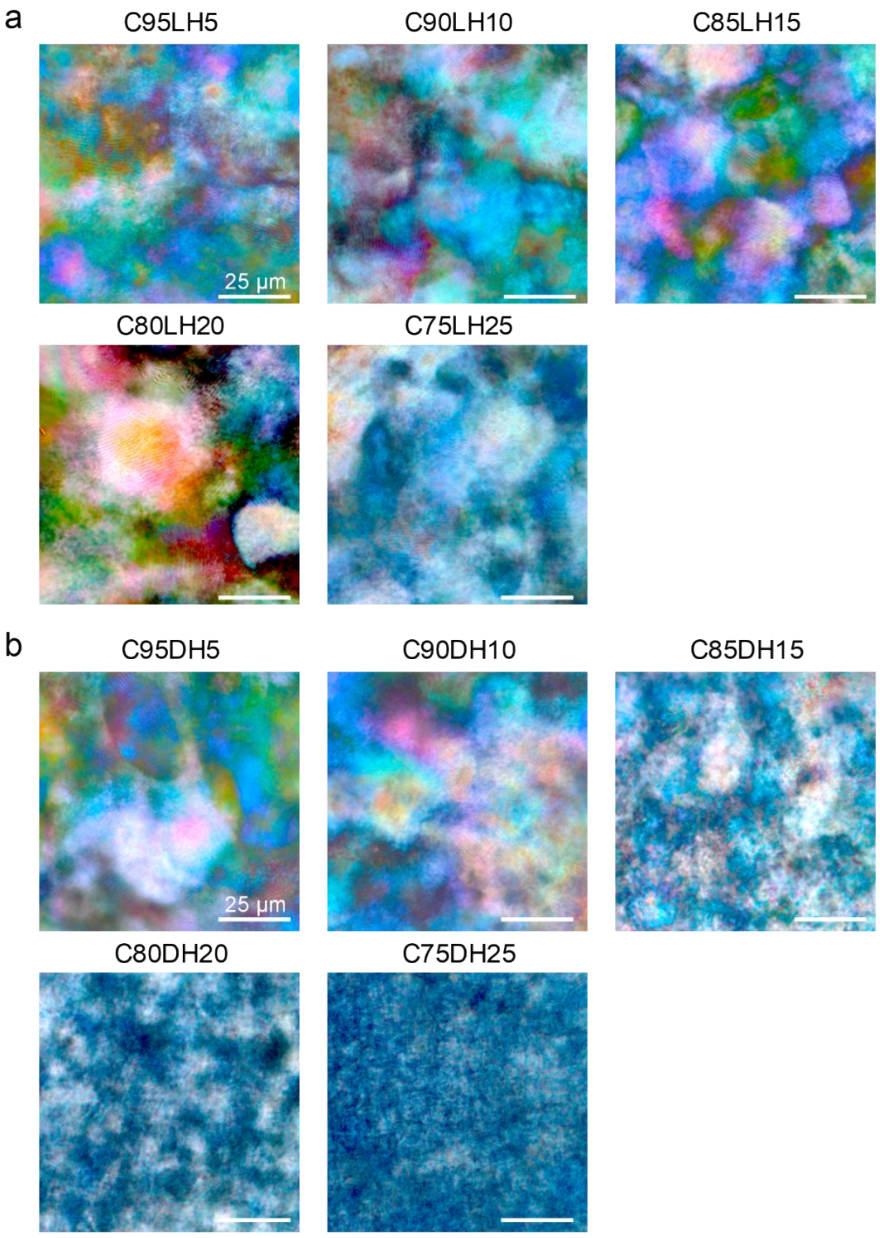

Figure S4. POM images of CNC/His hybrid films at varying concentrations. (a) $_{L}$-His series. (b) $_{D}$-His series. All the scale bars are 25 μm.

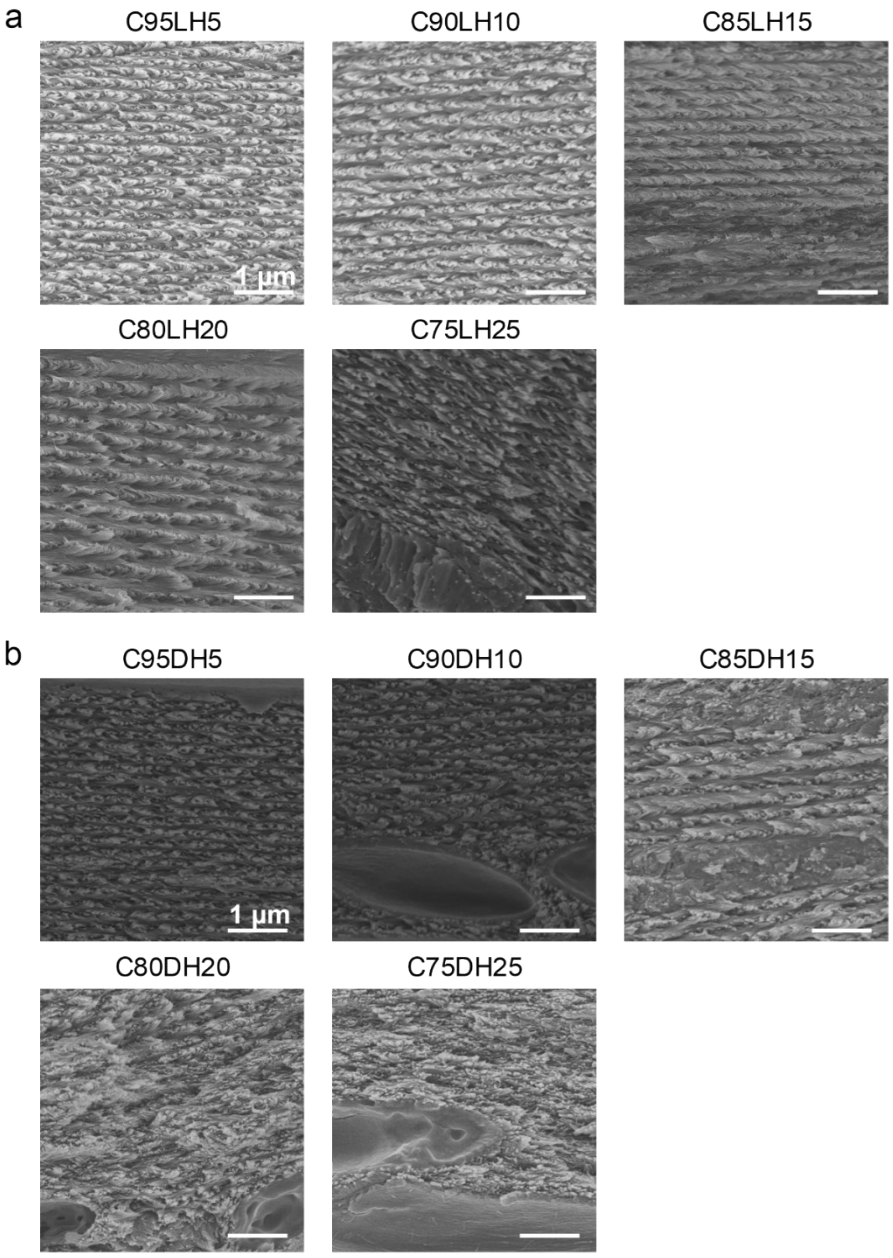

Figure S5. Crossing sectional SEM images of CNC/His hybrids films at varying concentrations. (a) $_{L}$-His series. (b) $_{D}$-His series. All the scale bars are 1 μm.

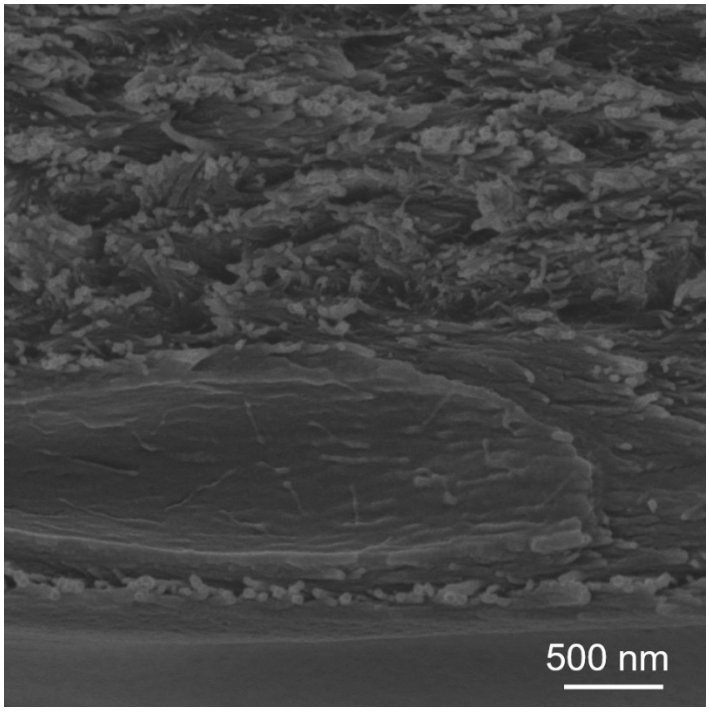

Figure S6. Crossing sectional SEM image of C90DH10 film, showing a large crystal of $_{D}$-histidine was mixed with some CNC rods.

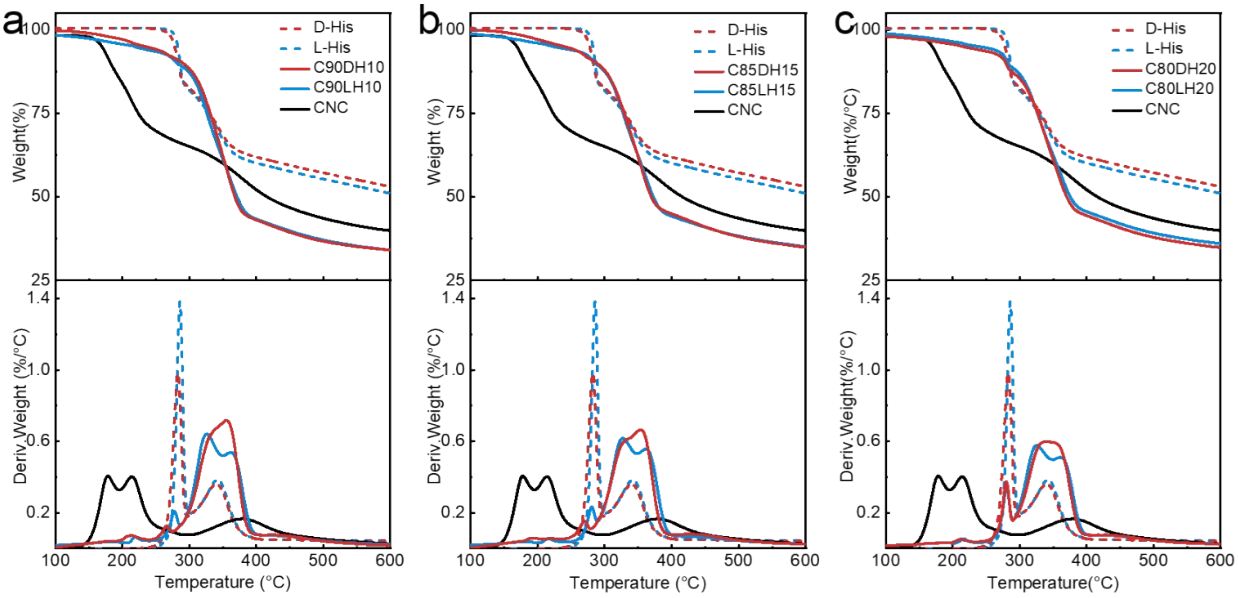

Figure S7. TGA (upper) and DTGA (bottom) curves of CNC, $_{L}$-His, $_{D}$-His, CxLHy, and CxDHy.

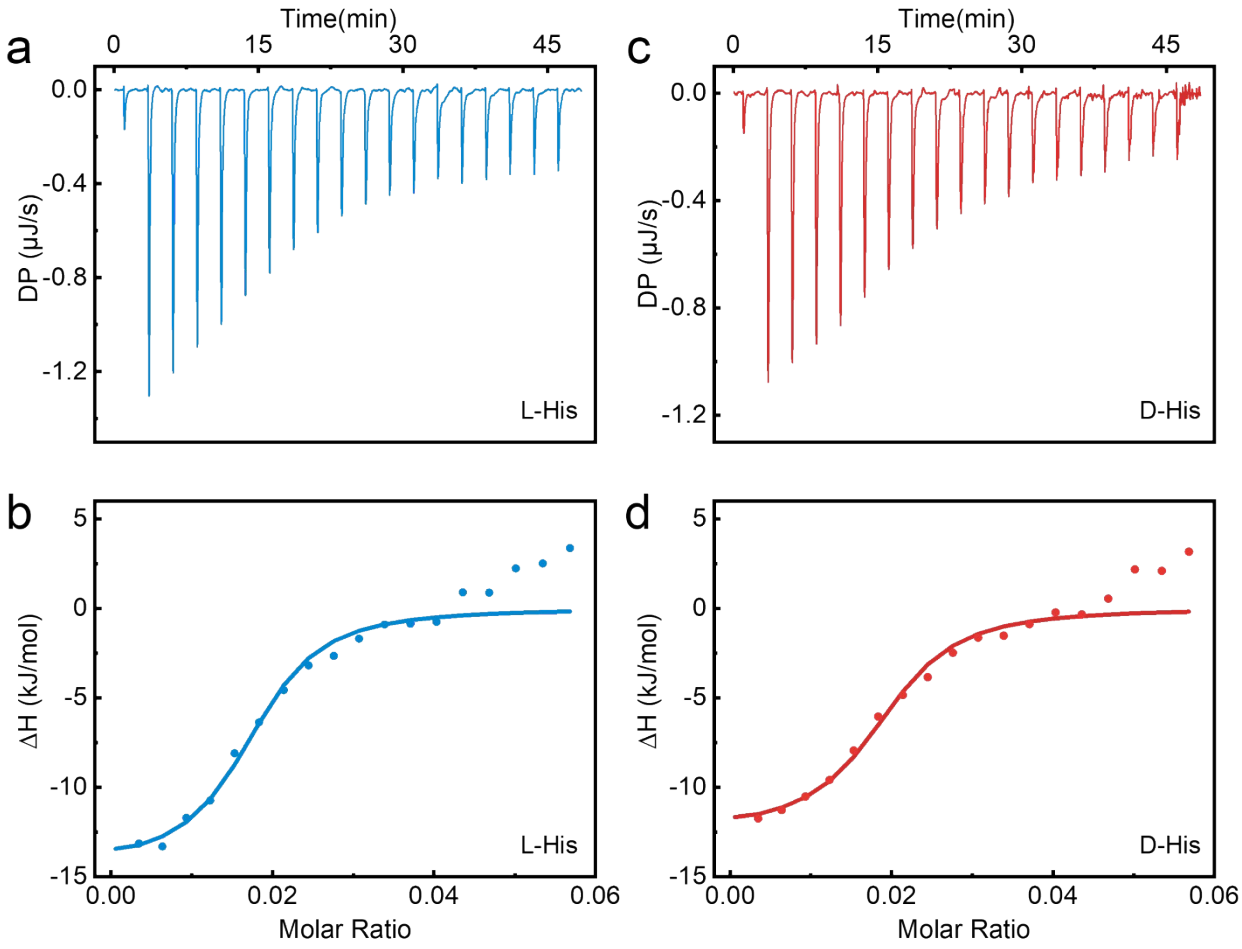

Figure S8. ITC titration curves of CNCs suspension with adding histidine (a, b: $_{L}$-His; c, d: $_{D}$-His). The data points, which did not coincide with the fitting curves, were supposed from the second titration process where the histidine anions (accepted two protons) were further neutralized by the excess amino acid.

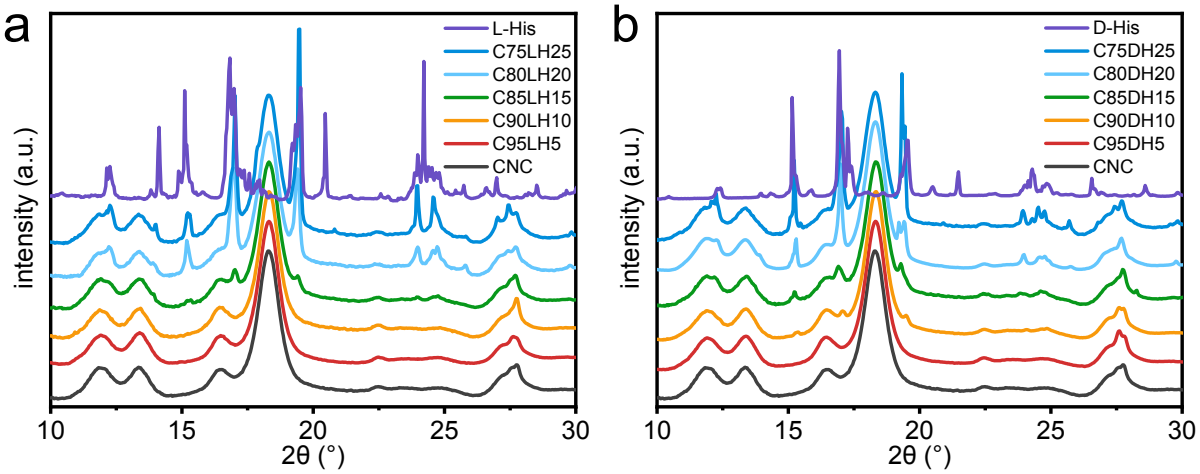

Figure S9. Synchrotron radiation WAXS curves of CNC/His hybrid films. The grain size of histidine in different composite films was calculated based on the Debye-Scherrer formula and listed in Table S3.

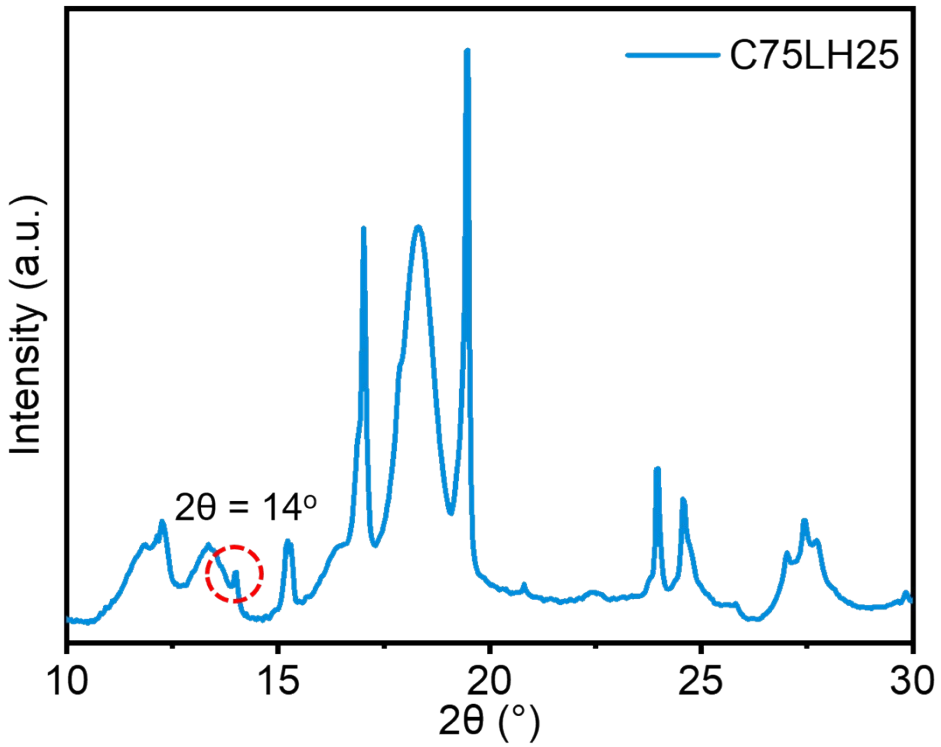

Figure S10. Synchrotron radiation WAXS curves of sample C75LH25, recorded at the beamline BL16B1 of the Shanghai Synchronization Radiation Facility, with the wavelength of 0.124 nm. A small sharp peak highlighted with the red dash circle at around 14.0° appears. It corresponds to the characteristic peak of $_{L}$-His's orthorhombic crystalline form (17.6° obtained by using Cu Kα radiation). [4] Thus, we deduced that $_{L}$-His preferred to crystalize into orthorhombic form under the existence of CNCs and have chosen it as the 3-dimension model for further discussion.

Table S1. Composition of CNC/$_{L}$-His or $_{D}$-His films.

Sample	The mass ratio (CNCs: His)
CNC	100:0
C99.5LH0.5/ C99.5DH0.5	99.5: 0.5
C99LH1/ C99DH1	99: 1
C98LH2/C98DH2	49: 1
C96LH4/C96DH4	24: 1
C95LH5/C95DH5	19: 1
C90LH10/C90DH10	9: 1
C85LH15/C85DH15	17: 3
C80LH20/C80DH20	4: 1
C75LH25/C75DH25	3: 1
C50LH50/C50DH50	1: 1
C25LH75/C25DH75	1: 3

Table S2. Thermodynamic parameters obtained from the ITC titration.

Chiral probe	$_{L}$-His	$_{D}$-His
ΔH (kJ/mol)	-14.4 ± 1.6	-12.5 ± 1.3
-TΔS (kJ/mol)	-19.5	-21.3
ΔG (kJ/mol)	-33.9	-33.7
N * (sites)	$1.7\times10^{-2} \pm 1.4\times10^{-3}$	$1.9\times10^{-2} \pm 1.5\times10^{-3}$

According to this result, in the mixing process of $_{L}$-His/$_{D}$-His with CNC, the thermodynamic difference was marginal, within the range of error.

*Sites values (N) mean the contents of the sulfonic group. Here the ITC results show that CNCs of this batch contains 1.8 sulfonic groups per 100 glucose units.

Table S3. The grain size of histidine in the composite films calculated based on the Debye-Scherrer formula.

Sample	***hkl***	Grain size(nm)	Sample	***hkl***	Grain size(nm)
C85LH15	(004)	24.64	C85DH15	(080)	40.81

	(110)	27.09		(111)	20.76
	(020)	24.96		(200)	40.00
C80LH20	(004)	29.61	C80DH20	(080)	54.71
	(110)	22.83		(111)	45.74
	(020)	30.26		(200)	78.56
C75LH25	(004)	25.12	C75DH25	(080)	47.20
	(110)	54.18		(111)	46.41
	(020)	55.79		(200)	87.15

With the increasing amount of histidine in films, the thickness of most planes gradually grew up. And compared the samples with the same weight percent of histidine, the average crystalline size of $_{L}$-His was much smaller than that of $_{D}$-His.

Video S1. Recording of the drying process of the drop-cast C80LH20 suspension under Polarized optical microscope. This video was recorded under a 100× magnification and at a 60× playback speed.
Video S2. Recording of the drying process of the drop-cast C80DH20 suspension under Polarized optical microscope. This video was recorded under a 100× magnification and at a 60× playback speed.

Reference :

1 J. G. Mesu, T. Visser, F. Soulimani and B. M. Weckhuysen, *Vib. Spectrosc.*, 2005, **39**, 114-125.
2 S. Martusevičius, G. Niaura, Z. Talaikyté and V. Razumas, *Vib. Spectrosc.*, 1996, **10**, 271-280.
3 M. N. Fukuya, K. Senoo, M. Kotera, M. Yoshimoto and O. Sakata, *Biomacromolecules*, 2017, **18**, 4411-4415.
4 L. Wantha, N. Punmalee, V. Sawaddiphol and A. E. Flood, *J. Cryst. Growth*, 2018, **490**, 65-70.